Research Article

Altered hACE2 binding affinity and S1/S2 cleavage efficiency of SARS-CoV-2 spike protein mutants affect viral cell entry

Ke Wang [a,b,c], Yu Pan [a], Dianbing Wang [a], Ye Yuan [a], Min Li [a], Yuanyuan Chen [a], Lijun Bi [a], Xian-En Zhang [a,b,c,*]

[a] National Key Laboratory of Biomacromolecules, Institute of Biophysics, Chinese Academy of Sciences, Beijing, 100101, China
[b] Faculty of Synthetic Biology, Shenzhen Institute of Advanced Technology, Shenzhen, 518055, China
[c] University of Chinese Academy of Sciences, Beijing, 100101, China

ARTICLE INFO

ABSTRACT

SARS-CoV-2 variants are constantly emerging, hampering public health measures in controlling the number of infections. While it is well established that mutations in spike proteins observed for the different variants directly affect virus entry into host cells, there remains a need for further expansion of systematic and multifaceted comparisons. Here, we comprehensively studied the effect of spike protein mutations on spike expression and proteolytic activation, binding affinity, viral entry efficiency and host cell tropism of eight variants of concern (VOC) and variants of interest (VOI). We found that both the full-length spike and its receptor-binding domain (RBD) of Omicron bind to hACE2 with an affinity similar to that of the wild-type. In addition, Alpha, Beta, Delta and Lambda pseudoviruses gained significantly enhanced cell entry ability compared to the wild-type, while the Omicron pseudoviruses showed a slightly increased cell entry, suggesting the vastly increased rate of transmission observed for Omicron variant is not associated with its affinity to hACE2. We also found that the spikes of Omicron and Mu showed lower S1/S2 cleavage efficiency and inefficiently utilized TMPRSS2 to enter host cells than others, suggesting that they prefer the endocytosis pathway to enter host cells. Furthermore, all variants' pseudoviruses we tested gained the ability to enter the animal ACE2-expressing cells. Especially the infection potential of rats and mice showed significantly increased, strongly suggesting that rodents possibly become a reservoir for viral evolution. The insights gained from this study provide valuable guidance for a targeted approach to epidemic control, and contribute to a better understanding of SARS-CoV-2 evolution.

1. Introduction

Severe acute respiratory syndrome coronavirus 2 (SARS-CoV-2) is the causative agent of the ongoing coronavirus pandemic (COVID-19). To date, over 600 million cases globally have been confirmed, with conservative estimates of approximately 6.6 million deaths due to infections with SARS-CoV-2 (WHO, 2022a). SARS-CoV-2 infects host cells following an interaction between the receptor binding domain (RBD) of viral spike (S) protein on the virus surface and the membrane-distal portion of angiotensin converting enzyme 2 (ACE2) on the surface of a variety of host cells, including lung, kidney, cardiovascular and intestinal systems, etc. (V'kovski et al., 2021).

With the widespread and continuous evolution of SARS-CoV-2, multiple variants are constantly emerging. A selected number of these variants constitute the major driving forces behind the global COVID-19 pandemic, including Alpha (B.1.1.7), Beta (B.1.351), Gamma (P.1), Delta (B.1.617.2) and Omicron (B.1.1.529), which therefore have been designated as VOC. Of these variations, Alpha, Beta, and Delta successively dominated the past three waves of epidemic peaks (He et al., 2021). Omicron is now causing the fourth wave. Except for VOCs, variants such as Lambda (C.37) and Mu (B.1.621) were listed as VOI based on their epidemiological traits (WHO, 2022b). The main driver of SARS-CoV-2 spread is the transmission from human to human. However, it appears that animal cases infected with SARS-CoV-2 are on the rise (Sharun et al., 2021). For example, four unidentified SARS-CoV-2 strains in sewer samples from New York City infected mice and rats (Smyth et al., 2022), while the Delta variant infected hamsters in Hong Kong in early 2022 (Miot et al., 2022). As of October 2022, nearly 700 outbreaks in animals involving 26 species (e.g. cats, dogs, mink, otters, hamsters) have been reported in 36 countries (Oie, 2022). It is imperative to closely monitor

the transmission of SARS-CoV-2 among animals and remain vigilant for any possible evolution that may occur within animal hosts.

The spike protein formed a corolla-like structure in a homotrimer form and is cleaved into two fragments S1 and S2 by a furin protease (Xing et al., 2022). The S1/S2 cleavage changes the conformation of the spike protein, which is then further cleaved by type II transmembrane serine protease (TMPRSS2) at the S2′ cleavage site, thus facilitating membrane fusion. SARS-CoV-2 enters host cells by two pathways: membrane fusion mediated by TMPRSS2 and endosomal entry activated by Cathepsin L (Lu et al., 2015; Jackson et al., 2022; Takeda, 2022). The critical step of viral entry into host cells requires interaction between the viral spike protein and the host receptor ACE2. Mutations in spike protein have been characterized for their effects on binding kinetics, entry efficiency and immune escape. For example, the N501Y mutation in RBD enhances the binding affinity to ACE2, which causes an increase in transmission of the Alpha variant (Liu Y. et al., 2022). The E484K mutation in the Beta, Gamma, Mu, and Omicron lineages reduces the effect of neutralizing antibodies in serum and improves the immune escape ability of variants (Altmann et al., 2021). The P681 mutation in Omicron affects the spike protein cleavage. As a result, Omicron prefers to enter cells via the endocytosis pathway (Du et al., 2022; Meng et al., 2022). Multiple amino acid mutations in Omicron spike protein few affect the binding of RBD with hACE2, but significantly increase the viral immune escape ability (Cameroni et al., 2022; Mannar et al., 2022). In addition, recent studies evaluated the influence of RBD mutants on the recognition and binding with ACE2 orthologs from animal species, strongly suggesting that cross-species infectivity and transmissibility of SARS-CoV-2 is feasible (Ren W.et al., 2022; Zhang et al., 2022a).

Although different research groups use different approaches to characterize the multitude of existing variants (Starr et al., 2020; Freer et al., 2021; Laffeber et al., 2021; Mohammadi et al., 2021; Ren S.Y. et al., 2022), there remains a need for systematic and multifaceted comparison of the biophysical traits of these variants. In this study, we systematically examined and compared the effects of spike protein mutations from six VOCs and two VOIs, including Alpha, Beta, Gamma, Delta, Omicron BA.1 (Nextstrain clade 21K, also termed B.1.1.529), Omicron BA.2 (Nextstrain clade 21L), Lambda and Mu, using the spike protein mutants and their RBD regions of SARS-CoV-2, as well as pseudoviruses. Our study provides comprehensive information that is critical for better evaluating the differences in transmissibility and cross-species transmission of these SARS-CoV-2 variants.

2. Materials and methods

2.1. Vector construction

Plasmid expressing the original strain SARS-CoV-2 spike protein (pcDNA3.1-S-WT, HG-VJH1153) was purchased from Honorgene (Hunan, China). Plasmids encoding the full-length spike gene of the Alpha (B.1.1.7), Beta (B.1.351), Gamma (P.1), Delta (B.1.617.2), Omicron (BA.1), Omicron (BA.2), Lambda (C.37), and Mu (B.1.621) variants were generated by site-directed overlap extension PCR using pcDNA3.1-S-WT as the template. All SARS-CoV-2 genome sequences used in this study were downloaded from GISAID (https://www.gisaid.org/) and these constructs codon were optimised. The variation characteristics in spike protein of SARS-CoV-2 VOCs and VOIs mutation information were shown in Fig. 1.

To construct the expression plasmids for RBD mutants (Arg319–Phe541) of SARS-CoV-2 variants, the RBD mutant fragment was subcloned from the corresponding pcDNA3.1-S plasmid and inserted in pcDNA3.1 (+) (Addgene plasmid# V790-20) with a preceding signal peptide and a C-terminal 10× histidine tag. To measure the expression of spike protein, the gene encoding spike protein mutants was fused with mCherry at the C-terminal and cloned into PiggyBac Dual Promoter plasmid (PB513B-1, Fenghui, Hunan, China) to generate the

series of PB513B-1-S plasmids. All spike genes were subcloned from the corresponding pcDNA3.1-S plasmid. Lentivirus (HIV-1)-based three plasmid systems, including psPAX2 (Addgene plasmid#12260), pLVX-Luc-T2A-GFP and pcDNA3.1-S, were used to produce pseudovirus. To construct pLVX-Luc-T2A-GFP, pLVX-T2A-mCherry-Puro (courtesy of Chen Chang, Institute of Biophysics, CAS, Beijing) was digested with *Bam*HI and *Mlu*I and insert the DNA fragments of luciferase and GFP using homologous recombination. The cDNAs encoding the ACE2 orthologs were synthesized by Sangon Biotech (Beijing, China) and cloned into the PB513B-1 vector to construct stable cell lines expressing different ACE2s. The cDNAs encoding TMPRSS2 were synthesized by Sangon and cloned into the pLVX-T2A-mCherry-Puro to produce lentivirus with the TMPRSS2 gene. All constructs were verified by Sanger sequencing.

2.2. Cell culture

Human embryonic kidney 293T cells (HEK293T) and their derivative cell lines, including 293T-hACE/TMPRSS2, 293T-mACE2/TMPRSS2, 293T-RatACE2/TMPRSS2, 293T-RhACE2/TMPRSS2, 293T-odACE2/TMPRSS2, were maintained in Dulbecco's Modified Eagle Medium (DMEM, Gibco) supplemented with 10% fetal bovine serum (FBS, Gibco) at 37 °C and 5% CO_2. Human colon cancer cells (Caco-2) were maintained in Eagle's Minimum Essential Medium (EMEM, Sigma-Aldrich) with 20% fetal bovine serum. Expi293F suspension cells (Thermo Fisher) were maintained in StarFect 293 Transient Transfection Medium (Genstar, Beijing, China) at 37 °C in a humidified 8% CO_2 incubator rotating at 130 rpm. Cells were tested routinely and confirmed to be free of mycoplasma contamination.

2.3. Stable cell line construction

The stable cell lines expressing human ACE2, mouse ACE2, rat ACE2, rhesus ACE2 and white-tailed deer ACE2 were generated by co-transfecting PA210PA-1 vector (Fenghui, Hunan, China) and the corresponding ACE2 orthologs PB200PA-1 vectors into HEK293T cells and puromycin selection applied for 10 days (4 μg/mL). Stable cell lines expressing both ACE2 orthologs and TMPRSS2 were constructed by infecting corresponding ACE2 orthologs stable cell lines with lentiviruses expressing TMPRSS2 and sorted by FACSAria IIIu (BD Biosciences). The lentiviruses expressing TMPRSS2 were produced by transient co-transfection of the third-generation packaging plasmids pMD2.G (Addgene plasmid#12259), psPAX2 and the pLVX-TMPRSS2-T2A-mCherry with Lipofectamine 3000 (Thermo Fisher Scientific) into HEK293T cells.

2.4. Production of SARS-CoV-2 pseudovirus and determination of viral entry efficiency

To prepare pseudoviruses with spike protein of SARS-CoV-2 variants, HEK293T cells at ~80% confluence in a 10 cm dish were transfected with 7 μg of psPAX2, 7 μg of pLVX-Luc-T2A-GFP, and 6 μg of S protein expression plasmid using Lipofectamine 3000 according to the manufacturer's protocol. After 48 h of transfection, the supernatants were harvested and passed through a 0.45 μm filter (Millipore) to remove cell debris, and stored at −80 °C. Moreover, HIV-1 p24 protein was quantitated using a p24 ELISA kit (Key-Bio Biotech, Beijing, China) following the manufacturer's instruction. Virus entry was assessed by transduction pseudoviruses in target cells in 96-well plates. The cells (20,000 cells/100 μL) were seeded in 96-well plates. The next day, pseudovirus preparations normalized for viral capsid p24 levels were added to cells. After 6 h post-transduction, cell supernatant was replaced with fresh medium and then cells were incubated for 48 h. Cells were then lysed and intracellular luciferase activity was determined using the luciferase assay system (Beyotime, Shanghai, China)
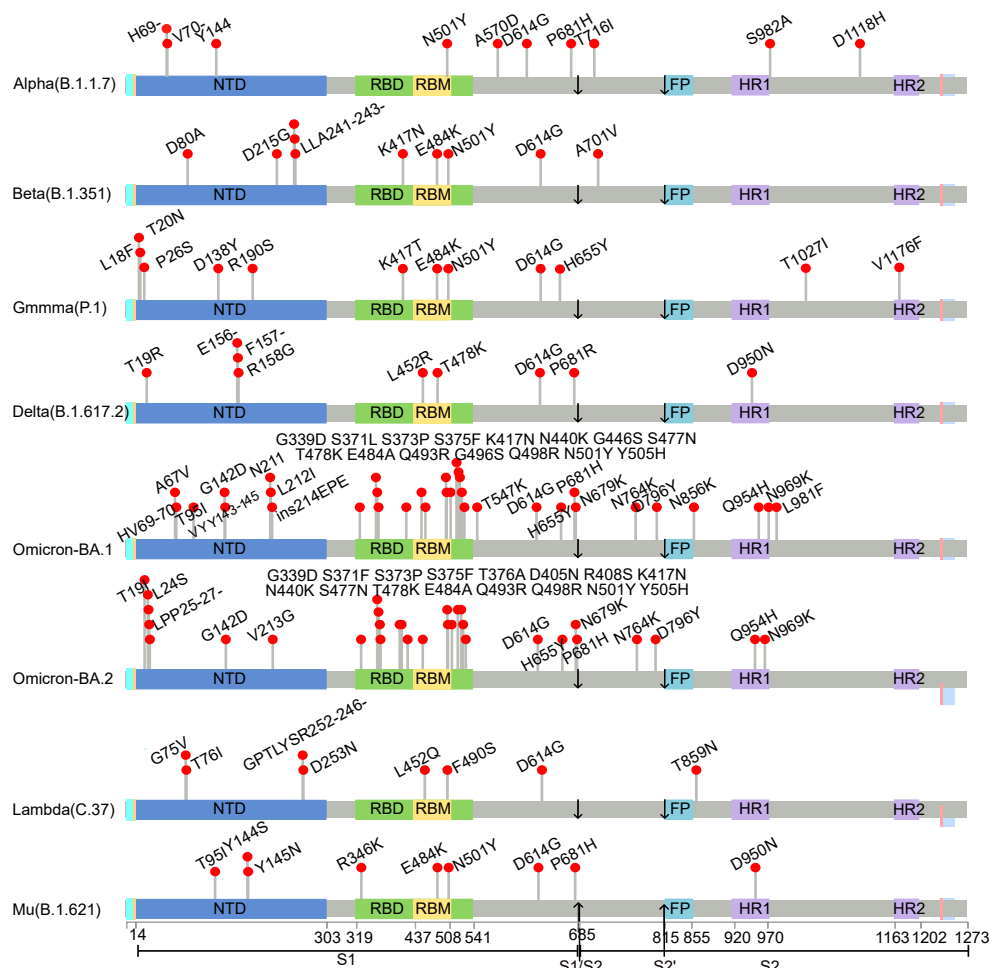
Fig. 1. Schematic overview of spike protein mutations of SARS-CoV-2 variants. The amino acid mutation sites in spike proteins are highlighted by red dots. The furin cleavage sites (S1/S2) and TMPRSS2 cleavage site (S2′) are indicated by arrows. NTD, N-terminal domain; RBD, receptor-binding; RBM, receptor-binding motif; FP, fusion peptide; HR1, heptad repeat 1; HR2, heptad repeat 2.

according to the manufacturer's specifications. All these experiments were performed in BSL-2 laboratories.

2.5. Expression and purification of SARS-CoV-2 RBD

Expi293F cells were diluted to 1.5×10^6 cells/mL before transfection. Next, 50 μg of RBD constructs were transfected into 50 mL suspension Expi293F with StarFect high-efficiency transfection reagent (Genstar, Beijing, China). Following 4 days of culturing by shaking, media were collected and centrifuged to harvest the supernatant and cleared of debris by 0.45-μm filtration before loading onto a 1 mL HisTrap excel column (Cytiva). The column was washed for 5 column volumes (CVs) with wash buffer (0.2 mol/L PBS, pH = 8.0), and 5 CVs of wash buffer supplemented with 20 mmol/L imidazole to equilibrate the column. Next, samples were loaded in equilibration buffer (0.2 mol/L PBS, pH = 8.0, with 20 mmol/L imidazole), after that, protein was eluted with elution buffer (0.2 mol/L PBS, pH = 8.0, 500 mmol/L imidazole). Elution fractions containing the protein were collected for SDS-PAGE validation. Elution buffer was then changed with PBST (0.2 mol/L, 0.05% tween-20, pH = 8.0) for desalting and concentration using Amicon ultrafiltration devices (Millipore, 10 kDa). The protein concentrations of purified samples were determined based on BSA standard curve protein quantification method using BCA Protein Content Assay Kit (Beyotime, Shanghai, China). Protein samples were flash-frozen in liquid nitrogen and stored at −80 °C.

2.6. Surface plasmon resonance (SPR)

SPR measurements were performed on a Biacore 8K (GE Healthcare Life Sciences) at 25 °C using PBST (0.2 mol/L, pH = 8.0) as Running buffer. Protein A chip (Cytiva) was used and ACE2-hFc (SinoBiological, 10108-H02H) at a concentration of 10 μg/mL as a ligand was captured to ~150 RU on the chip surface through Fc tag. Spike mutant proteins (Acrobiosystem, Being, China) and RBD mutant proteins flow through the chip surface as analytes. A concentration series with two-fold dilutions (200 nmol/L, 100 nmol/L, 50 nmol/L, 25 nmol/L, 12.5 nmol/L, 6.75 nmol/L, 3.125 nmol/L and 0 nmol/L) of analytes were injected using a multi-cycle method. SARS-CoV-2 spike RBD mutants were injected into Fc1-Fc2 of the channel at a flow rate of 30 μL/min for an association phase of 60 s, followed by 300 s dissociation. SARS-CoV-2 spike protein mutants were injected at a flow rate of 30 μL/min for an association phase of 180 s, followed by 900 s dissociation. The association and dissociation are all processed in the Running Buffer.

Eight cycles were repeated according to the sample concentration from low to high. At the end of each analysis cycle, the sensor chip surface was completely regenerated using Glycine 1.5 (Cytiva) as injection buffer to remove ligand and analyte at a flow rate of 20 μL/min for 30 s. Biacore 8K Control Software 2.0.1 (Cytiva) was used to collect data and Biacore X100 Evaluation Software 2.0.1 (Cytiva) was used to analyze data. Calculation of association (k_a) and dissociation (k_d) rate constants

was based on a 1:1 Langmuir binding model. The equilibrium dissociation constant (K_D) was calculated from k_d/k_a.

2.7. Spike protein mutants expression detection

To detect the expression of spike protein mutants, HEK293T cells were transfected with the series of Tr-S-mCherry-EF1a-GFP plasmids with lipofectamine 3000. 24 h post-transfection, the cells were collected and washed twice with cold PBS. Cells were then subjected to FACSAria IIIu (BD Biosciences) analysis to detect the mean fluorescence signal intensity of mCherry and GFP, the ratio of red to the green fluorescence intensity of cells indicated the relative expression of spike protein mutants.

2.8. Western blot analysis

Samples were diluted with $5\times$ sample buffer (Genstar, Beijing, China) and boiled for 10 min. Samples were then separated on a 10% SDS-PAGE and transferred to a PVDF membrane. After blocking the non-specific sites with 5% (w/v) skim milk, the membranes were incubated with the primary antibody, followed by the HRP-conjugated secondary antibody. Western blot was used to analyze the spike protein cleavage. For cell lysate, HEK293T cells were transfected with the spike protein expressing plasmids. The cells were collected and lysed by RIPA Lysis Buffer (Beyotime, Shanghai, China) after 24 h. The lysates were centrifugated (12,000 rpm for 10 min at 4 °C) and supernatants were collected. For pseudovirus (PV) particles, the collected PVs were concentrated by ultra-filtrated using an Amicon Ultra-4 centrifugal filter device (Millipore, 100 kDa) for analysis.

The following primary antibodies were used: mouse anti-SARS-CoV-2 spike protein antibody (Sino Biological, Cat: 40592-MM117), mouse anti-HIV-1 p24 protein monoclonal antibody (Sino Biological, Cat: 11695-MM15), and mouse anti-GAPDH antibody (Abcam, ab8245). HRP-linked goat anti-mouse IgG (Abcam, ab6789) and HRP-linked goat anti-rabbit IgG (Abcam, ab6721) were used as the secondary antibodies. The cleavage ratio of S2 to full-length spike protein was measured by densitometry using ImageJ.

2.9. Statistical analysis

Data analysis were conducted using GraphPad Prism version 9.0.0. All results are expressed as the means $\pm$ standard deviations. The statistical significance of between-group differences was analyzed using t-tests or one-way analysis of variance (ANOVA). P values less than 0.05 were considered to be statistically significant. ****, $P < 0.0001$; ***, $P < 0.001$; **, $P < 0.01$; *, $P < 0.05$; not significant ($P > 0.05$); P values less than or equal to 0.05 were displayed. If not otherwise stated, the mean value of three technical replicates was used for quantification assays.

3. Results

3.1. Expression and S1/S2 cleavage efficiency of SARS-CoV-2 spike protein variants

Characteristics of the different spike protein mutant forms of SARS-CoV-2 selected in this study are shown in Fig. 1. To determine the expression of spike proteins, mCherry was inserted at the C-terminal of spike gene and driven by a CMV promoter for fusion expression. As a control, we used the EFa1 promotor to initiate the expression of GFP. The fluorescence intensity was measured by flow cytometry, and the ratio of mCherry/GFP was used to evaluate the spike protein expression. As shown in Fig. 2A, only Delta spike protein (S-Delta) showed significantly increased mCherry signal compared with the wild type strain (S-WT).

The S1/S2 cleavage of spike protein results in a conformational change, which is essential for the virus to enter the host cells through membrane fusion. As the mutations in the cleavage site presumably affect the proteolytic processing, we analyzed the cleavage efficiency of spike protein mutants in S1/S2 site. We first produced pseudovirus (PVs) with variants' spike proteins and analyzed the cleavage bands of these proteins using Western blot. As shown in Fig. 2B and C, two bands appeared on the blot, one for full-length spike protein (S0) and one for the product (S2) cleaved by furin. The cleaved bands of S-Omicron-BA.1, S-Omicron-BA.2 and S-Mu were weaker than that of S-WT. To assess the cleavage during spike protein synthesis, we further lysed the cells transfected spike proteins expressing plasmids and analyzed the proteins in the cell lysate. We found that in Omicron-BA.1, Omicron-BA.2 and Mu, cleavage of spike proteins was greatly reduced compared to the WT control (Fig. 2D and E).

3.2. Affinity and kinetics of spike protein mutants binding to hACE2

To investigate how our RBD mutants interact with hACE2, we expressed recombinant RBD proteins harboring either single or combined mutations in 293F cells (Supplementary Fig. S1). We then measured hACE2 binding affinities of the purified mutant forms using surface plasmon resonance (SPR) biosensor (Supplementary Table S1; Fig. 3A and C). We found that only RBD-Omicron exhibited a similar affinity to that for RBD-WT, while the other RBD mutants exhibited an increase in hACE2 binding affinity. In addition, hACE2 binding of RBD-Alpha, RBD-Gamma and RBD-Lambda were 7.29-, 6.06-, and 10.43-fold stronger than that of RBD-WT, respectively. When we analyzed our single mutant forms, we found that mutation N501Y (RBD-Alpha) resulted in the greatest (7.29-fold) effect on the binding affinity, decreasing the k_d by 6.54-fold. Mutation of L452R increased the affinity 4.86-fold, by increasing the k_a by 6.65-fold, while E484K/Q mutation slightly increased the affinity (1.52–1.77-fold). Although the single mutation N501Y (7.29-fold) and L452R (4.86-fold) significantly enhance the affinities of their RBD mutants, the combined mutations E484K + N501Y (1.53-fold), E484Q + L452R (0.7-fold) and T478K + L452R (RBD-Delta, 1.65-fold) showed decreased binding affinity relative to individual mutations. Presumably, this observed decrease is a result of the T478K and E484 site mutations. On the contrary, the hACE2 affinity of K417N/T + E484K + N501Y (RBD-Beta, 3.36-fold; RBD-Gamma, 6.06-fold) combinations, indicate the intricate effects of combinatorial mutations.

To examine the effect of non-RBD mutations on the interaction between spike protein and hACE2, we further compared the binding affinity of full-length spike protein mutants to hACE2 (Supplementary Table S2; Fig. 3B and D). The S-Alpha mutant form showed the strongest hACE2 binding, reaching a 6.15-fold increase in affinity compared to S-WT. The S-Mu mutant form showed a 5.83-fold increase in binding affinity, with a 9.24-fold decrease in k_d value. In comparison, we found no significant increase in binding affinity for the mutant forms S-Beta, S-Gamma, S-Delta and S-Lambda; S-Omicron exhibited reduced hACE2 binding affinity.

In addition, we noted that the binding affinity of S-WT (1.00 nmol/L) was far higher (21.8-fold) than hACE2 affinity of RBD-WT (21.8 nmol/L). Moreover, all full-length spike protein mutants exhibited enhancement of binding affinity compared to their corresponding RBD mutants (Supplementary Table S1 and Table S2). Together, these results strongly suggested that non-RBD of spike protein also plays a key importance in the binding of spike protein with hACE2. Furthermore, the spike protein mutations in the non-RBD of the different variants showed varying effects on the binding affinity. For example, while the RBD-Lambda mutation increased hACE2 binding by over 10-fold compared to RBD-WT, the S-Lambda mutation only showed a slight increase in binding (1.33-fold) compared to S-WT. In addition, the binding affinity of RBD-Mu increased less (2.4-fold) than that of the S-Mu mutant (5.83-fold). Together, these results show that the mutations of spike protein either in the RBD or in the non-RBD affect the interaction of the virus with host cells.
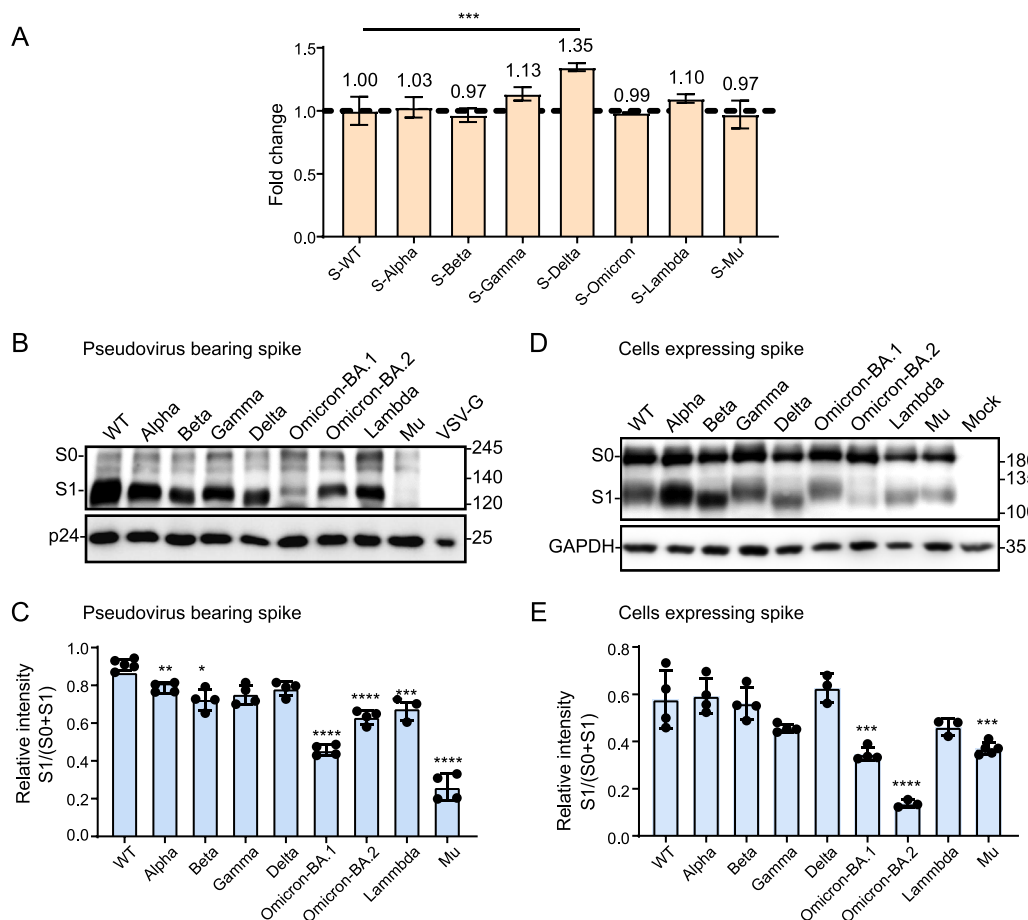
Fig. 2. Expression and S1/S2 cleavage efficiency of SARS-CoV-2 variants' spike proteins. **A** Expression of SARS-CoV-2 variants' spike proteins in 293T cells. mCherry fluorescence intensity indicates spike protein expression, and GFP fluorescence intensity is the reference control. The fluorescence intensity ratio of mCherry/GFP indicates the relative expression level. The Y axis was normalized with S-WT fluorescence intensity ratio value. The numbers labeled on the bars indicate the average fold change of variants' spike protein expression relative to the S-WT. Omicron indicates BA.1 sublineage (also termed B.1.1.529) here. **B**, **C** Spike protein cleavage of pseudovirus (PVs) of the WT and variants probed with antibody against RBD. HIV-1 p24 was used to normalize the protein sample loading. **D**, **E** S1/S2 cleavage efficiency of SARS-CoV-2 spikes. The spike proteins of WT and variants were expressed in HEK293T cells and at 48 h post-transfection, cell lysates were made for Western blot analysis using the antibody against RBD. GAPDH served as the loading control. Full-length spike (S0) and S1 proteins are indicated. The ratio of S1 to the total spike was quantitatively analyzed using ImageJ. Data represent the mean ± SD of 3–5 independent replicates. Significance was analyzed by one-way ANOVA. P values less than 0.05 were considered to be statistically significant. ****, $P < 0.0001$; ***, $P < 0.001$; **, $P < 0.01$; *, $P < 0.05$; ns, not significant ($P > 0.05$).

3.3. Cell entry efficiency of SARS-CoV-2 spike-bearing pseudovirus variants

To determine the effect of spike protein mutations on the ability of the virus entry into host cells, we prepared nine kinds of pseudoviruses expressing the spike proteins from ancestral strain, Alpha (B.1.1.7), Beta (B.1.351), Gamma (P.1), Delta (B.1.617.2), Omicron (B.1.1.529), Omicron (BA.2), Lambda (C.37), and Mu (B.1.621) using a lentiviral three-plasmid packing system. As p24 protein is a highly expressed structural protein of the lentivirus, the titers of various PVs were determined by quantification of p24 using enzyme linked immunosorbent assay (ELISA). Next, we used the normalized amounts of PVs to infect 293T cells overexpressing hACE2 (293T-hACE2), 293T cells overexpressing hACE2 and TMPRSS2 (293T-hACE2-TMPRSS2) and intestinal epithelial Caco-2 cells (expressing hACE2 and TMPRSS2) (Fig. 4 and Supplementary Fig. S2). Fig. 4A showed that the cell entry efficacy of PV-Beta (24.6-fold) and PV-Lambda (7.6-fold) was significantly higher ($P < 0.0001$) than that of PV-WT, and PV-Alpha showed a 4.6-fold higher ($P < 0.01$) increase in 293T-hACE2 cells. In addition,

PV-Gamma, PV-Delta, PV-Omicron-BA.1 and PV-Omicron-BA.2 displayed a slight (2.8–3.4-fold) increase in entry. However, PV-Mu exhibited a reduced entry ability (0.4-fold).

In Caco-2 cells, PV-Alpha, PV-Beta, PV-Delta and PV-Lambda gained a greatly increased (12.2–40-fold) entry ability compared to PV-WT. In comparison, PV-Omicron only exhibited a small increase (1.8–2.4-fold). PV-Mu exhibited a decrease in entry efficiency (0.2-fold). When we repeated these experiments in 293-hACE2-TMPRSS2 cells, we found that entry efficiencies exhibited a comparable trend in Caco-2 cells, demonstrating that spike protein mutations from Alpha, Beta, Gamma, Delta and Lambda all increase the abilities for virus entering host cells. In addition, PV-Gamma and PV-Delta exhibited similar cell entry abilities in 293-hACE2 cells, but that of PV-Delta was higher (2.5–3.8-fold) than PV-Gamma in the TMPRSS2 expressing cells (293-hACE2-TMPRSS2 and Caco-2), suggesting that TMPRSS2 increases cell entry of PV-Delta. Furthermore, we found the PV variants, except PV-Omicron and PV-Mu, exhibited higher entry ability in the TMPRSS2 expressing cells than in the cells without TMPRSS2 (Fig. 4B), indicating that Omicron and Mu fail to efficiently use TMPRSS2. Overall, these results demonstrated
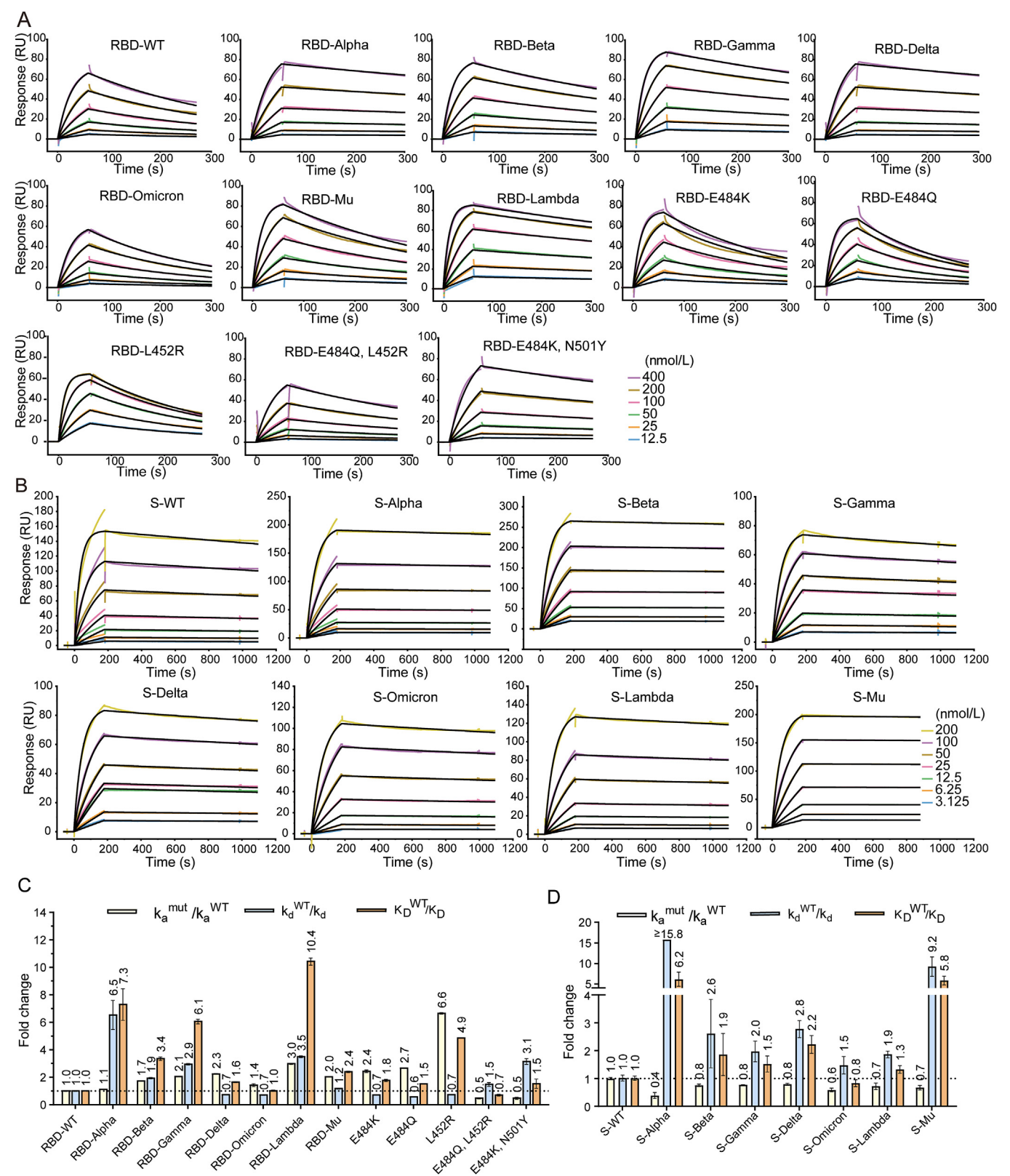
Fig. 3. SPR analysis of the interaction between SARS-CoV-2 variants' spike proteins and hACE2. **A** Representative traces of muti-cycle kinetic analyses of RBD mutants bearing single and combined mutations to hACE2 binding. **B** Representative traces of muti-cycle kinetic analyses of full-length spike protein mutants to hACE2 binding. The raw data (colored) is fit (black) to a model using a 1:1 Langmuir binding. **C, D** The fold change of the calculated KD, k_a, and k_d for binding of (**C**) the indicated RBD mutants and (**D**) full-length spike protein mutants to hACE2 relative to that of WT. Data represent the mean ± SD of 3 independent replicates. Omicron indicates BA.1 sublineage (also termed B.1.1.529) here. k_a, association rate constant; k_d, dissociation rate; KD, equilibrium dissociation constant; KD = k_d/k_a.
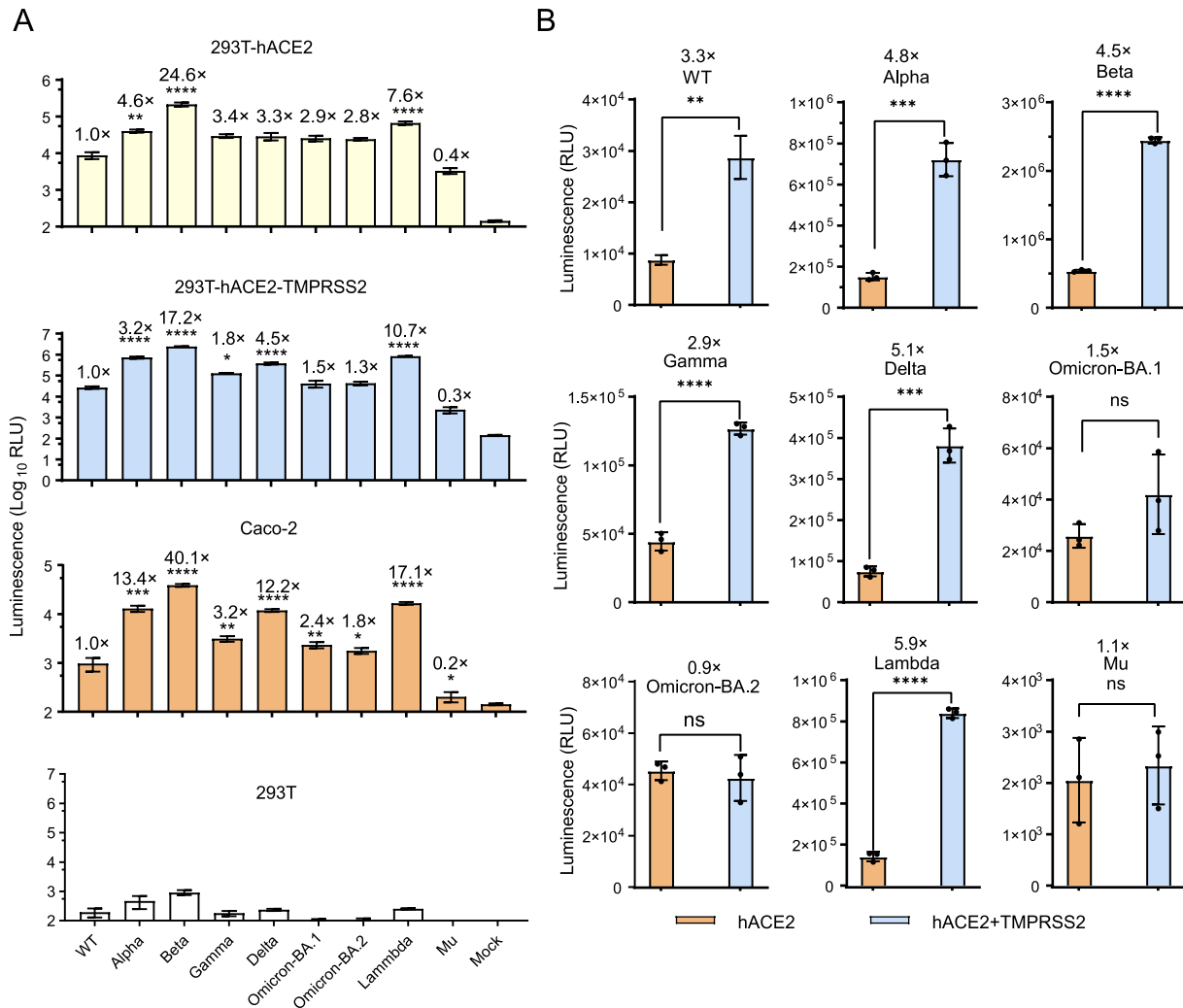
Fig. 4. Cell entry ability of SARS-CoV-2 pseudotyped variants bearing mutate spike proteins. **A** The ability of SARS-CoV-2 pseudotyped variants entering into 293T-hACE2 cells (only expressing hACE2), 293T-hACE2-TMPRSS2 cells (co-expressing hACE2 and TMPRSS2), Caco-2 cells (co-expressing hACE2 and TMPRSS2) and 293T cells (expressing low hACE2). **B** Entry comparison of pseudotyped variants in cells overexpressing hACE2 and TMPRSS2 or without TMPRSS2. HIV-1 p24 was used to normalize the PVs' additive does, and the data was calculated at 5 ng p24. The numbers labeled on the bars indicate (**A**) the average fold change of PV variants relative to the PV-WT or (**B**) the average fold change of 293T-hACE2-TMPRSS2 cells relative to 293T-hACE2 cells. Data are mean ± SD of 3 independent replicates. Mock, uninfected control (no virus); P values less than 0.05 were considered to be statistically significant. ****, $P < 0.0001$; ***, $P < 0.001$; **, $P < 0.01$; *, $P < 0.05$; ns, not significant ($P > 0.05$). Significance was analyzed by (**A**) one-way ANOVA or (**B**) t-test.

that the mutations in spike protein alter the usage of TMPRSS2 and the ability of the virus to enter the host cells.

3.4. Cross species tropism of SARS-CoV-2 spike-bearing pseudovirus variants

To determine the influence of spike protein mutations on host tropism, we evaluated the susceptibilities of 293T cells expressing ACE2 orthologs of human (hACE2), mouse (mACE2), rat (ratACE2), rhesus (rhACE2), and white-tailed deer (*Odocoileus virginianus*) (odACE2) to these nine types of PVs, respectively. As shown in Fig. 5, cells expressing rhACE2 were susceptible to infection by PV-WT, with an efficiency approximately 4-fold higher than that of hACE2. PV-Beta and PV-Alpha displayed a significantly increased entry efficiency into 293T-mACE2, 293T-ratACE2 and 293T-rhACE2 cells. PV-Beta (51–99-fold) and PV-Alpha (17–25-fold) also more efficiently enter into the above-

mentioned cells than PV-WT enter into 293T-hACE2 cells. In addition, PV-Gamma, PV-Delta, PV-Omicron-BA.1, PV-Omicron-BA.2, and PV-Mu infected cells expressing either mACE2 or ratACE2, with an approx. 1.5–8-fold higher infectivity than PV-WT infects 293T-hACE2 cells.

Furthermore, we evaluated the entry efficiency of these pseudoviruses in cell lines by coexpressing TMPRSS2 and various ACE2 orthologs. We found that all variants' pseudoviruses exhibited increased cell entry ability in TMPRSS2+ cells expressing ACE2 of either mouse, rat or rhesus origin. These results are in agreement with our results from 293T-hACE2-TMPRSS2 cells. In addition, we found that efficiencies in cell entry of PV-Omicron-BA.1, PV-Omicron-BA.2 and PV-Mu differed little between TMPRSS2+ and TMPRSS2- cells, indicating that the mutations in S-Omicron and S-Mu impact the TMPRSS2 utilization of these two strains. Together, our findings demonstrate that the mutations in the spike protein result in the susceptibility of animal host cells to SARS-CoV-2 variants.
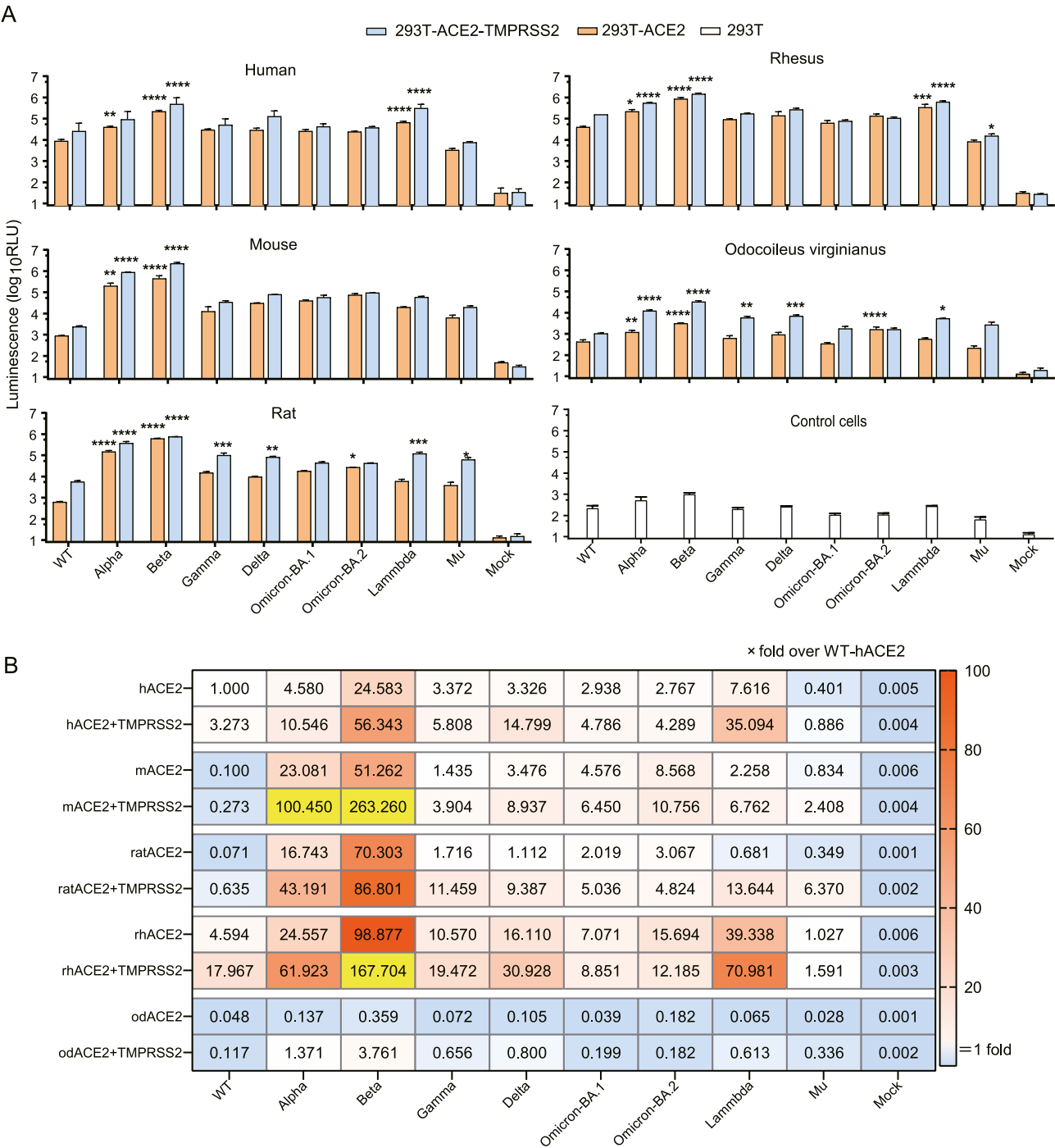
Fig. 5. Cross-species infection of SARS-CoV-2 pseudotyped variants bearing mutate spike proteins. **A** The ability of SARS-CoV-2 pseudotyped variants entering into cells expressing ACE2 orthologs of human, mouse, mouse, rat, rhesus, *Odocoileus virginianus* and with TMPRSS2 (blue columns) or without (orange columns). **B** A heatmap shows the fold change of the cross-species infection performance of PV variants. The Control group is the ability of PV-WT to enter into 293T-hACE2 cells. The color bar represents the scale. HIV-1 p24 was used to normalize the PVs' additive does, and the data was calculated at 5 ng p24. Data are mean $\pm$ SD of 3–4 replicates (four for Mu, and three for others) and were normalized to the WT of the individual experiment. Mock, uninfected control (no virus); P values less than 0.05 were considered to be statistically significant. ****, $P < 0.0001$; ***, $P < 0.001$; **, $P < 0.01$; *, $P < 0.05$; ns, not significant ($P > 0.05$). Significance was analyzed by one-way ANOVA.

4. Discussion

Here, we revealed that the spike protein mutations affect the spike protein expression, S1/S2 cleavage, and the binding to hACE2, which result in varying cell entry efficiency and the host tropism of SARS-CoV-2 variants.

Spike protein is a critical structural component of SARS-CoV-2 particles. Our results revealed that the expression level of the Delta strain's spike protein is higher than that of other strains. We infer that the heightened expression of S-Delta potentially provides more materials for virion assembly, thereby inducing increased virus production. So we speculate the high expression of spike protein is one of the reasons for the

observed high viral load in Delta-infected patients (Li et al., 2022). Nonetheless, it is important to acknowledge that there are various factors influencing viral load, such as viral uncoating, RNA replication, budding, etc.

Recent studies demonstrated that the weaker cleavage of S-Omicron is lower than that of S-WT and S-Delta (Du et al., 2022; Iwata-Yoshi-kawa et al., 2022; Meng et al., 2022; Zhang et al., 2022b). We showed that the S1/S2 cleavage in S-Omicron-BA.1, S-Omicron-BA.2 and S-Mu were significantly reduced compared with S-WT, which possibly is due to their P681H mutation within the furin cleavage site (Lubinski et al., 2022). However, S-Alpha carrying P681H mutation showed a similar proportion of cleaved spike protein with S-WT. These results suggested that the mutations surrounding the furin cleavage site (e.g., T716I) also regulate the furin-mediated cleavage of spike protein. The mutations in spike protein impact the furin cleavage both during spike protein synthesis and viral assembly, but the concentration of cleaved fragments in the cell lysate was lower than that in PVs. Presumably, this reduction is caused by the fact that viral assembly prefers to utilize the cleaved spike proteins rather than full-length spike proteins or spike proteins are cleaved during the exocytosis release of virions (V'kovski et al., 2021; Meng et al., 2022).

Spike protein undergoes S1/S2 cleavage by furin or furin-like proteases during virus maturation in infected cells or viral initial entry into host cells extracellularly. Furin preactivation causes the "close" spike protein conformation to an "open" conformation for efficiently binding to the host cell receptor. After virus bound to ACE2, the conformation of S1 subunit was changed and the S2′ cleavage site in the S2 subunit was exposed, then the S2′ cleavage by TMPRSS2 occurs to facilitate membrane fusion at the cell surface (Hoffmann et al., 2020). Alternatively, the viral particles can also enter host cells by lysosomal cathepsin L mediated endocytosis (Bayati et al., 2021). Single virion imaging also showed that SARS-CoV-2 virions enter four kinds of respiratory cells by endocytosis in our previous report (Ma et al., 2021). Considering S2′ cleavage is based on the conformational changes induced by S1/S2 cleavage, we hypothesize that the weaker suboptimal S1/S2 cleavage in spike protein mutants causes inefficient S2′ processing and insufficient fusion peptide exposure, resulting in impaired TMPRSS2 usage. Our results indicated that TMPRSS2 is not required for Omicron-BA.1, Omicron-BA.2 and Mu to promote pseudovirus entry. Presumably, the main entry path for Omicron and Mu into host cells is endocytosis. Together, these findings may explain why Omicron replicates fast in cells of the upper airway which are characterized by low expression of TMPRSS2, compared to other variants (Salahudeen et al., 2020; Fan et al., 2022; Hui et al., 2022; Meng et al., 2022; Shuai et al., 2022; Zhao et al., 2022).

The binding ability of SARS-CoV-2 variants' spike proteins and their RBD regions with hACE2 is a controversial topic. Several studies showed that the binding ability of RBD-Omicron or S-Omicron to hACE2 is marginally higher than that of WT (Cameroni et al., 2022; Cui et al., 2022; Mannar et al., 2022), but other reports showed that Omicron failed to show increased binding affinity with hACE2 (Han et al., 2022; Wu et al., 2022; Zheng et al., 2022). The most likely explanation for these discrepancies is the differences in experimental materials or methods (Fan et al., 2022). Therefore, we conducted a systematic comparative experiment, and the results led us to conclude that, compared with WT, the binding ability of Omicron spike protein as well as its RBD region to hACE2 did not increase. Together, the mutations in S-Omicron showed little effect on receptor recognition and binding to hACE2.

Furthermore, we found that the binding affinity of RBDs to hACE2 and viral cell entry efficiency has a positive correlation. The PV-Omicron-BA.1 and PV-Omicron-BA.2 and PV-Mu failed to gain significantly increased cell entry efficacy compared to PV-WT. Given that existence of the furin cleavage site in the spike protein is crucial for SARS-CoV-2 high infectivity (Benton et al., 2020; Wrobel et al., 2020; Wu et al., 2020), the most likely explanation for weaker cell entry of Omicron and Mu pseudoviruses is the inefficient furin cleavage due to the mutations in S1/S2

cleavage site. In despite of it, Omicron variants have extremely high transmissibility (Long et al., 2022; Pulliam et al., 2022; Viana et al., 2022). Strong evidences indicate that the immune escape ability is primarily responsible for the increased infectivity of Omicron variants (Zhang et al., 2021; Altarawneh et al., 2022; Cameroni et al., 2022; Cao et al., 2022; Dejnirattisai et al., 2022; Kuhlmann et al., 2022; Liu L. et al., 2022; Neil Ferguson et al., 2022). In addition, the immuno-escaping ability of Mu has also been reported (Laiton-Donato et al., 2021; Halfmann et al., 2022b; Pascarella et al., 2022).

In addition, we found that all the variants' pseudoviruses extend their usage of ACE2 orthologs to mice, rats, rhesus, and white-tailed deer, suggesting that the variants gain the ability to infect animal cells. These results are in agreement with previous studies. Several studies reported that Omicron variants cause attenuated disease in mice (Wei et al., 2021; Halfmann et al., 2022a) and suggested that rodents should be considered as a threat to the cross-species transmission of SARS-CoV-2 variants (Huang et al., 2021; Ren W. et al., 2022). In addition, SARS-CoV-2 antibodies were found in white-tailed deer, suggesting that SARS-CoV-2 efficiently transmits between white-tailed deer species (Chandler et al., 2021; Palmer et al., 2021; Hale et al., 2022; Kuchipudi et al., 2022; Martins et al., 2022). Together, all these results imply that as the host changes from human to animal or vice versa, SARS-CoV-2 continues to evolve, resulting in novel mutant forms emerging. Therefore, investigating the transmission of variants in wild animal populations is critical to the origin-tracing of SARS-CoV-2.

While our study has clearly demonstrated that the spike protein mutations affect the host cell entry and host-tropism of SARS-CoV-2 VOCs and VOIs pseudoviruses, it has some limitations that merit consideration in future research. We performed infection assays using pseudoviruses based on the lentiviral system, which carries the SARS-CoV-2 spike protein gene instead of the SARA-CoV-2 genome. Although the protocol is effective for assessing viral cell entry function, it cannot be used to study the subsequent molecular events of SARS-CoV-2 variants. In addition, we used the human cells expressing animals' ACE2 orthologs to evaluate the cross-tropism potentials of variants. However, it is necessary to utilize animal cells for fully assessing the complex mechanisms responsible for cross-species virus transmission.

5. Conclusions

In summary, we provide here a comprehensive evaluation of the relationship between spike protein mutations and viral infectivity in SARS-CoV-2 variants. Compared with the WT strain, both spike proteins and their RBDs of all SARS-CoV-2 variants, except Omicron, showed increased binding affinities to hACE2; Alpha, Beta, Delta, and Lambda variants (pseudoviruses) exhibited obviously increased cell entry ability, while Mu pseudoviruses are decreased. Omicron variant showed similar RBD-hACE2 binding affinity and slightly increased cell entry ability compared with WT strain, which implies that the significantly increased transmission rate of Omicron variants is not related to spike protein-hACE2 interaction. Furthermore, all variants' pseudoviruses gain the ability to use animal ACE2 for host cell entering, suggesting they have the potential for cross-species spillover. These findings could be as references for future investigation on the infection and pathogenic mechanisms of the SARS-CoV-2 variant strains, and be helpful to answer the public concerns about the related issues.

Data availability

All the data generated during the current study are included in the manuscript.

Ethics statement

All experiments with SARS-CoV-2 pseudovirus were conducted in a biosafety level 2 (BSL2) facility in the IBP, CAS.

Author contributions

Ke Wang: conceptualization, data curation, formal analysis, investigation, methodology, resources, validation, writing-original draft. Yu Pan: data curation, investigation, resources, validation. Dianbing Wang: funding acquisition, methodology, project administration, resources, validation, writing-review & editing. Ye Yuan: resources, validation. Min Li: project administration, resources. Yuanyuan Chen: methodology, resources, validation. Lijun Bi: resources, supervision. Xian-En Zhang: conceptualization, formal analysis, funding acquisition, investigation, methodology, resources, supervision, validation, writing-original draft, writing-review & editing.

Conflict of interest

The authors have declared that no competing interest exists.

Acknowledgments

Appendix A. Supplementary data

Supplementary data to this article can be found online at https://doi.org/10.1016/j.virs.2023.06.005.

References

Altarawneh, H.N., Chemaitelly, H., Hasan, M.R., Ayoub, H.H., Qassim, S., Almukdad, S., Coyle, P., Yassine, H.M., Al-Khatib, H.A., Benslimane, F.M., Al-Kanaani, Z., Al-Kuwari, E., Jeremijenko, A., Kaleeckal, A.H., Latif, A.N., Shaik, R.M., Abdul-Rahim, H.F., Nasrallah, G.K., Al-Kuwari, M.G., Butt, A.A., Al-Romaihi, H.E., Al-Thani, M.H., Al-Khal, A., Bertollini, R., Tang, P., Abu-Raddad, L.J., 2022. Protection against the Omicron variant from previous SARS-CoV-2 infection. N. Engl. J. Med. 386, 1288–1290.

Altmann, D.M., Boyton, R.J., Beale, R., 2021. Immunity to SARS-CoV-2 variants of concern. Science 371, 1103–1104.

Bayati, A., Kumar, R., Francis, V., Mcpherson, P.S., 2021. SARS-CoV-2 infects cells after viral entry via clathrin-mediated endocytosis. J. Biol. Chem. 296, 100306.

Benton, D.J., Wrobel, A.G., Xu, P., Roustan, C., Martin, S.R., Rosenthal, P.B., Skehel, J.J., Gamblin, S.J., 2020. Receptor binding and priming of the spike protein of SARS-CoV-2 for membrane fusion. Nature 588, 327–330.

Cameroni, E., Bowen, J.E., Rosen, L.E., Saliba, C., Zepeda, S.K., Culap, K., Pinto, D., Vanblargan, L.A., De Marco, A., Di Iulio, J., Zatta, F., Kaiser, H., Noack, J., Farhat, N., Czudnochowski, N., Havenar-Daughton, C., Sprouse, K.R., Dillen, J.R., Powell, A.E., Chen, A., Maher, C., Yin, L., Sun, D., Soriaga, L., Bassi, J., Silacci-Fregni, C., Gustafsson, C., Franko, N.M., Logue, J., Iqbal, N.T., Mazzitelli, I., Geffner, J., Grifantini, R., Chu, H., Gori, A., Riva, A., Giannini, O., Ceschi, A., Ferrari, P., Cippa, P.E., Franzetti-Pellanda, A., Garzoni, C., Halfmann, P.J., Kawaoka, Y., Hebner, C., Purcell, L.A., Piccoli, L., Pizzuto, M.S., Walls, A.C., Diamond, M.S., Telenti, A., Virgin, H.W., Lanzavecchia, A., Snell, G., Veesler, D., Corti, D., 2022. Broadly neutralizing antibodies overcome SARS-CoV-2 Omicron antigenic shift. Nature 602, 664–670.

Cao, Y., Wang, J., Jian, F., Xiao, T., Song, W., Yisimayi, A., Huang, W., Li, Q., Wang, P., An, R., Wang, J., Wang, Y., Niu, X., Yang, S., Liang, H., Sun, H., Li, T., Yu, Y., Cui, Q., Liu, S., Yang, X., Du, S., Zhang, Z., Hao, X., Shao, F., Jin, R., Wang, X., Xiao, J., Wang, Y., Xie, X.S., 2022. Omicron escapes the majority of existing SARS-CoV-2 neutralizing antibodies. Nature 602, 657–663.

Chandler, J.C., Bevins, S.N., Ellis, J.W., Linder, T.J., Tell, R.M., Jenkins-Moore, M., Root, J.J., Lenoch, J.B., Robbe-Austerman, S., Deliberto, T.J., Gidlewski, T., Kim Torchetti, M., Shriner, S.A., 2021. SARS-CoV-2 exposure in wild white-tailed deer (Odocoileus virginianus). Proc. Natl. Acad. Sci. U. S. A. 118.

Cui, Z., Liu, P., Wang, N., Wang, L., Fan, K., Zhu, Q., Wang, K., Chen, R., Feng, R., Jia, Z., Yang, M., Xu, G., Zhu, B., Fu, W., Chu, T., Feng, L., Wang, Y., Pei, X., Yang, P., Xie, X.S., Cao, L., Cao, Y., Wang, X., 2022. Structural and functional characterizations of infectivity and immune evasion of SARS-CoV-2 Omicron. Cell 185, 860–871.e. 13.

Dejnirattisai, W., Shaw, R.H., Supasa, P., Liu, C., Stuart, A.S., Pollard, A.J., Liu, X., Lambe, T., Crook, D., Stuart, D.I., Mongkolsapaya, J., Nguyen-Van-Tam, J.S., Snape, M.D., Screaton, G.R., Com, C.O.V.S.G., 2022. Reduced neutralisation of SARS-CoV-2 omicron B.1.1.529 variant by post-immunisation serum. Lancet 399, 234–236.

Du, X., Tang, H., Gao, L., Wu, Z., Meng, F., Yan, R., Qiao, S., An, J., Wang, C., Qin, F.X., 2022. Omicron adopts a different strategy from Delta and other variants to adapt to host. Signal Transduct. Target. Ther. 7, 45.

Fan, Y., Li, X., Zhang, L., Wan, S., Zhang, L., Zhou, F., 2022. SARS-CoV-2 Omicron variant: recent progress and future perspectives. Signal Transduct. Target. Ther. 7, 141.

Freer, G., Lai, M., Quaranta, P., Spezia, P.G., Pistello, M., 2021. Evolution of viruses and the emergence of SARS-CoV-2 variants. New Microbiol. 44, 191–204.

Hale, V.L., Dennis, P.M., Mcbride, D.S., Nolting, J.M., Madden, C., Huey, D., Ehrlich, M., Grieser, J., Winston, J., Lombardi, D., Gibson, S., Saif, L., Killian, M.L., Lantz, K., Tell, R.M., Torchetti, M., Robbe-Austerman, S., Nelson, M.I., Faith, S.A., Bowman, A.S., 2022. SARS-CoV-2 infection in free-ranging white-tailed deer. Nature 602, 481–486.

Halfmann, P.J., Iida, S., Iwatsuki-Horimoto, K., Maemura, T., Kiso, M., Scheaffer, S.M., Darling, T.L., Joshi, A., Loeber, S., Singh, G., Foster, S.L., Ying, B., Case, J.B., Chong, Z., Whitener, B., Moliva, J., Floyd, K., Ujie, M., Nakajima, N., Ito, M., Wright, R., Uraki, R., Warang, P., Gagne, M., Li, R., Sakai-Tagawa, Y., Liu, Y., Larson, D., Osorio, J.E., Hernandez-Ortiz, J.P., Henry, A.R., Ciuoderis, K., Florek, K.R., Patel, M., Odle, A., Wong, L.R., Bateman, A.C., Wang, Z., Edara, V.V., Chong, Z., Franks, J., Jeevan, T., Fabrizio, T., Debeauchamp, J., Kercher, L., Seiler, P., Gonzalez-Reiche, A.S., Sordillo, E.M., Chang, L.A., Van Bakel, H., Simon, V., Consortium Mount Sinai Pathogen Surveillance Study, G., Douek, D.C., Sullivan, N.J., Thackray, L.B., Ueki, H., Yamayoshi, S., Imai, M., Perlman, S., Webby, R.J., Seder, R.A., Suthar, M.S., Garcia-Sastre, A., Schotsaert, M., Suzuki, T., Boon, A.C.M., Diamond, M.S., Kawaoka, Y., 2022a. SARS-CoV-2 Omicron virus causes attenuated disease in mice and hamsters. Nature 603, 687–692.

Halfmann, P.J., Kuroda, M., Armbrust, T., Theiler, J., Balaram, A., Moreno, G.K., Accola, M.A., Iwatsuki-Horimoto, K., Valdez, R., Stoneman, E., Braun, K., Yamayoshi, S., Somsen, E., Baczenas, J.J., Mitamura, K., Hagihara, M., Adachi, E., Koga, M., Mclaughlin, M., Rehrauer, W., Imai, M., Yamamoto, S., Tsutsumi, T., Saito, M., Friedrich, T.C., O'connor, S.L., O'connor, D.H., Gordon, A., Korber, B., Kawaoka, Y., 2022b. Characterization of the SARS-CoV-2 B.1.621 (Mu) variant. Sci. Transl. Med. 14, eabm4908.

Han, P., Li, L., Liu, S., Wang, Q., Zhang, D., Xu, Z., Han, P., Li, X., Peng, Q., Su, C., Huang, B., Li, D., Zhang, R., Tian, M., Fu, L., Gao, Y., Zhao, X., Liu, K., Qi, J., Gao, G.F., Wang, P., 2022. Receptor binding and complex structures of human ACE2 to spike RBD from omicron and delta SARS-CoV-2. Cell 185, 630–640. e10.

He, X., Hong, W., Pan, X., Lu, G., Wei, X., 2021. SARS-CoV-2 Omicron variant: characteristics and prevention. MedComm (2020) 2, 838–845.

Hoffmann, M., Kleine-Weber, H., Schroeder, S., Kruger, N., Herrler, T., Erichsen, S., Schiergens, T.S., Herrler, G., Wu, N.H., Nitsche, A., Muller, M.A., Drosten, C., Pohlmann, S., 2020. SARS-CoV-2 cell entry depends on ACE2 and TMPRSS2 and is blocked by a clinically proven protease inhibitor. Cell 181, 271–280.e8.

Huang, Y., Xie, J., Guo, Y., Sun, W., He, Y., Liu, K., Yan, J., Tao, A., Zhong, N., 2021. SARS-CoV-2: origin, intermediate host and allergenicity features and hypotheses. Healthcare (Basel) 9, 1132.

Hui, K.P.Y., Ho, J.C.W., Cheung, M.C., Ng, K.C., Ching, R.H.H., Lai, K.L., Kam, T.T., Gu, H., Sit, K.Y., Hsin, M.K.Y., Au, T.W.K., Poon, L.L.M., Peiris, M., Nicholls, J.M., Chan, M.C.W., 2022. SARS-CoV-2 Omicron variant replication in human bronchus and lung ex vivo. Nature 603, 715–720.

Iwata-Yoshikawa, N., Kakizaki, M., Shiwa-Sudo, N., Okura, T., Tahara, M., Fukushi, S., Maeda, K., Kawase, M., Asanuma, H., Tomita, Y., Takayama, I., Matsuyama, S., Shirato, K., Suzuki, T., Nagata, N., Takeda, M., 2022. Essential role of TMPRSS2 in SARS-CoV-2 infection in murine airways. Nat. Commun. 13, 6100.

Jackson, C.B., Farzan, M., Chen, B., Choe, H., 2022. Mechanisms of SARS-CoV-2 entry into cells. Nat. Rev. Mol. Cell Biol. 23, 3–20.

Kuchipudi, S.V., Surendran-Nair, M., Ruden, R.M., Yon, M., Nissly, R.H., Vandegrift, K.J., Nelli, R.K., Li, L., Jayarao, B.M., Maranas, C.D., Levine, N., Willgert, K., Conlan, A.J.K., Olsen, R.J., Davis, J.J., Musser, J.M., Hudson, P.J., Kapur, V., 2022. Multiple spillovers from humans and onward transmission of SARS-CoV-2 in white-tailed deer. Proc. Natl. Acad. Sci. U. S. A. 119, e2121644119..

Kuhlmann, C., Mayer, C.K., Claassen, M., Maponga, T., Burgers, W.A., Keeton, R., Riou, C., Sutherland, A.D., Suliman, T., Shaw, M.L., Preiser, W., 2022. Breakthrough infections with SARS-CoV-2 omicron despite mRNA vaccine booster dose. Lancet 399, 625–626.

Laffeber, C., De Koning, K., Kanaar, R., Lebbink, J.H.G., 2021. Experimental evidence for enhanced receptor binding by rapidly spreading SARS-CoV-2 variants. J. Mol. Biol. 433, 167058.

Laiton-Donato, K., Franco-Munoz, C., Alvarez-Diaz, D.A., Ruiz-Moreno, H.A., Usme-Ciro, J.A., Prada, D.A., Reales-Gonzalez, J., Corchuelo, S., Herrera-Sepulveda, M.T., Naizaque, J., Santamaria, G., Rivera, J., Rojas, P., Ortiz, J.H., Cardona, A., Malo, D., Prieto-Alvarado, F., Gomez, F.R., Wiesner, M., Martinez, M.L.O., Mercado-Reyes, M., 2021. Characterization of the emerging B.1.621 variant of interest of SARS-CoV-2. Infect. Genet. Evol. 95, 105038.

Li, B., Deng, A., Li, K., Hu, Y., Li, Z., Shi, Y., Xiong, Q., Liu, Z., Guo, Q., Zou, L., Zhang, H., Zhang, M., Ouyang, F., Su, J., Su, W., Xu, J., Lin, H., Sun, J., Peng, J., Jiang, H., Zhou, P., Hu, T., Luo, M., Zhang, Y., Zheng, H., Xiao, J., Liu, T., Tan, M., Che, R., Zeng, H., Zheng, Z., Huang, Y., Yu, J., Yi, L., Wu, J., Chen, J., Zhong, H., Deng, X., Kang, M., Pybus, O.G., Hall, M., Lythgoe, K.A., Li, Y., Yuan, J., He, J., Lu, J., 2022. Viral infection and transmission in a large, well-traced outbreak caused by the SARS-CoV-2 Delta variant. Nat. Commun. 13, 460.

Liu, L., Iketani, S., Guo, Y., Chan, J.F., Wang, M., Liu, L., Luo, Y., Chu, H., Huang, Y., Nair, M.S., Yu, J., Chik, K.K., Yuen, T.T., Yoon, C., To, K.K., Chen, H., Yin, M.T.,

Sobieszczyk, M.E., Huang, Y., Wang, H.H., Sheng, Z., Yuen, K.Y., Ho, D.D., 2022a. Striking antibody evasion manifested by the Omicron variant of SARS-CoV-2. Nature 602, 676–681.

Liu, Y., Liu, J., Plante, K.S., Plante, J.A., Xie, X., Zhang, X., Ku, Z., An, Z., Scharton, D., Schindewolf, C., Widen, S.G., Menachery, V.D., Shi, P.-Y., Weaver, S.C., 2022b. The N501Y spike substitution enhances SARS-CoV-2 infection and transmission. Nature 602, 294–299.

Long, B., Carius, B.M., Chavez, S., Liang, S.Y., Brady, W.J., Koyfman, A., Gottlieb, M., 2022. Clinical update on COVID-19 for the emergency clinician: presentation and evaluation. Am. J. Emerg. Med. 54, 46–57.

Lu, G., Wang, Q., Gao, G.F., 2015. Bat-to-human: spike features determining 'host jump' of coronaviruses SARS-CoV, MERS-CoV, and beyond. Trends Microbiol. 23, 468–478.

Lubinski, B., Fernandes, M.H.V., Frazier, L., Tang, T., Daniel, S., Diel, D.G., Jaimes, J.A., Whittaker, G.R., 2022. Functional evaluation of the P681H mutation on the proteolytic activation of the SARS-CoV-2 variant B.1.1.7 (Alpha) spike. iScience 25, 103589.

Ma, Y., Mao, G., Wu, G., Chen, M., Qin, F., Zheng, L., Zhang, X.E., 2021. Dual-fluorescence labeling pseudovirus for real-time imaging of single SARS-CoV-2 entry in respiratory epithelial cells. ACS Appl. Mater. Interfaces 13, 24477–24486.

Mannar, D., Saville, J.W., Zhu, X., Srivastava, S.S., Berezuk, A.M., Tuttle, K.S., Marquez, A.C., Sekirov, I., Subramaniam, S., 2022. SARS-CoV-2 Omicron variant: antibody evasion and cryo-EM structure of spike protein-ACE2 complex. Science 375, 760–764.

Martins, M., Boggiatto, P.M., Buckley, A., Cassmann, E.D., Falkenberg, S., Caserta, L.C., Fernandes, M.H.V., Kanipe, C., Lager, K., Palmer, M.V., Diel, D.G., 2022. From Deer-to-Deer: SARS-CoV-2 is efficiently transmitted and presents broad tissue tropism and replication sites in white-tailed deer. PLoS Pathog. 18, e1010197.

Meng, B., Abdullahi, A., Ferreira, I., Goonawardane, N., Saito, A., Kimura, I., Yamasoba, D., Gerber, P.P., Fatihi, S., Rathore, S., Zepeda, S.K., Papa, G., Kemp, S.A., Ikeda, T., Toyoda, M., Tan, T.S., Kuramochi, J., Mitsunaga, S., Ueno, T., Shirakawa, K., Takaori-Kondo, A., Brevini, T., Mallery, D.L., Charles, O.J., , Collaboration, C.-N.B.C.-., Genotype to Phenotype Japan, C., Ecuador, C.C., Bowen, J.E., Joshi, A., Walls, A.C., Jackson, L., Martin, D., Smith, K.G.C., Bradley, J., Briggs, J.A.G., Choi, J., Madissoon, E., Meyer, K.B., Mlcochova, P., Ceron-Gutierrez, L., Doffinger, R., Teichmann, S.A., Fisher, A.J., Pizzuto, M.S., De Marco, A., Corti, D., Hosmillo, M., Lee, J.H., James, L.C., Thukral, L., Veesler, D., Sigal, A., Sampaziotis, F., Goodfellow, I.G., Matheson, N.J., Sato, K., Gupta, R.K., 2022. Altered TMPRSS2 usage by SARS-CoV-2 Omicron impacts infectivity and fusogenicity. Nature 603, 706–714.

Miot, E.F., Worthington, B.M., Ng, K.H., De Lataillade, L.G., Pierce, M.P., Liao, Y., Ko, R., Shum, M.H., Cheung, W.Y., Holmes, E.C., Leung, K.S., Zhu, H., Poon, L.L., Peiris, M.J., Guan, Y., Leung, G.M., Wu, J.T., Lam, T.T., 2022. Surveillance of rodent pests for SARS-CoV-2 and other coronaviruses, Hong Kong. Emerg. Infect. Dis. 28, 467–470.

Mohammadi, M., Shayestehpour, M., Mirzaei, H., 2021. The impact of spike mutated variants of SARS-CoV2 [Alpha, Beta, Gamma, Delta, and Lambda] on the efficacy of subunit recombinant vaccines. Braz. J. Infect. Dis. 25, 101606.

Neil Ferguson, A.G., Cori, Anne, Hogan, Alexandra, Hinsley, Wes, Volz, Erik, on Behalf of the Imperial College Covid-19 Response Team, 2022. Report 49: Growth, population distribution and immune escape of Omicron in England [Online]. Imperial College London. Available: https://www.imperial.ac.uk/mrc-global-infectious-disease-ana lysis/covid-19/report-49-omicron/. (Accessed 12 June 2021).

Oie, 2022. SARS-CoV-2 in animals – Situation report 18 [Online]. World Organisation for Animal Health. Available: https://www.woah.org/en/document/sars-cov-2-in-an imals-situation-report-18/. (Accessed 11 July 2022).

Palmer, M.V., Martins, M., Falkenberg, S., Buckley, A., Caserta, L.C., Mitchell, P.K., Cassmann, E.D., Rollins, A., Zylich, N.C., Renshaw, R.W., Guarino, C., Wagner, B., Lager, K., Diel, D.G., 2021. Susceptibility of white-tailed deer (Odocoileus virginianus) to SARS-CoV-2. J. Virol. 95, e00083-21..

Pascarella, S., Bianchi, M., Giovanetti, M., Narzi, D., Cauda, R., Cassone, A., Ciccozzi, M., 2022. The SARS-CoV-2 Mu variant should not be left aside: it warrants attention for its immuno-escaping ability. J. Med. Virol. 94, 2479–2486.

Pulliam, J.R.C., Van Schalkwyk, C., Govender, N., Von Gottberg, A., Cohen, C., Groome, M.J., Dushoff, J., Mlisana, K., Moultrie, H., 2022. Increased risk of SARS-CoV-2 reinfection associated with emergence of Omicron in South Africa. Science 376, eabn4947.

Ren, S.Y., Wang, W.B., Gao, R.D., Zhou, A.M., 2022a. Omicron variant (B.1.1.529) of SARS-CoV-2: mutation, infectivity, transmission, and vaccine resistance. World J. Clin. Cases 10, 1–11.

Ren, W., Ju, X., Gong, M., Lan, J., Yu, Y., Long, Q., Kenney, D.J., O'connell, A.K., Zhang, Y., Zhong, J., Zhong, G., Douam, F., Wang, X., Huang, A., Zhang, R., Ding, Q., 2022b. Characterization of SARS-CoV-2 variants B.1.617.1 (Kappa), B.1.617.2 (Delta), and B.1.618 by cell entry and immune evasion. mBio 13, e0009922.

Salahudeen, A.A., Choi, S.S., Rustagi, A., Zhu, J., Van Unen, V., De La, O.S., Flynn, R.A., Margalef-Catala, M., Santos, A.J.M., Ju, J., Batish, A., Usui, T., Zheng, G.X.Y., Edwards, C.E., Wagar, L.E., Luca, V., Anchang, B., Nagendran, M., Nguyen, K., Hart, D.J., Terry, J.M., Belgrader, P., Ziraldo, S.B., Mikkelsen, T.S., Harbury, P.B., Glenn, J.S., Garcia, K.C., Davis, M.M., Baric, R.S., Sabatti, C., Amieva, M.R., Blish, C.A., Desai, T.J., Kuo, C.J., 2020. Progenitor identification and SARS-CoV-2 infection in human distal lung organoids. Nature 588, 670–675.

Sharun, K., Dhama, K., Pawde, A.M., Gortazar, C., Tiwari, R., Bonilla-Aldana, D.K., Rodriguez-Morales, A.J., De La Fuente, J., Michalak, I., Attia, Y.A., 2021. SARS-CoV-2 in animals: potential for unknown reservoir hosts and public health implications. Vet. Q. 41, 181–201.

Shuai, H., Chan, J.F., Hu, B., Chai, Y., Yuen, T.T., Yin, F., Huang, X., Yoon, C., Hu, J.C., Liu, H., Shi, J., Liu, Y., Zhu, T., Zhang, J., Hou, Y., Wang, Y., Lu, L., Cai, J.P., Zhang, A.J., Zhou, J., Yuan, S., Brindley, M.A., Zhang, B.Z., Huang, J.D., To, K.K., Yuen, K.Y., Chu, H., 2022. Attenuated replication and pathogenicity of SARS-CoV-2 B.1.1.529 Omicron. Nature 603, 693–699.

Smyth, D.S., Trujillo, M., Gregory, D.A., Cheung, K., Gao, A., Graham, M., Guan, Y., Guldenpfennig, C., Hoxie, I., Kannoly, S., Kubota, N., Lyddon, T.D., Markman, M., Rushford, C., San, K.M., Sompanya, G., Spagnolo, F., Suarez, R., Teixeiro, E., Daniels, M., Johnson, M.C., Dennehy, J.J., 2022. Tracking cryptic SARS-CoV-2 lineages detected in NYC wastewater. Nat. Commun. 13, 635.

Takeda, M., 2022. Proteolytic activation of SARS-CoV-2 spike protein. Microbiol. Immunol. 66, 15–23.

V'kovski, P., Kratzel, A., Steiner, S., Stalder, H., Thiel, V., 2021. Coronavirus biology and replication: implications for SARS-CoV-2. Nat. Rev. Microbiol. 19, 155–170.

Viana, R., Moyo, S., Amoako, D.G., Tegally, H., Scheepers, C., Althaus, C.L., Anyaneji, U.J., Bester, P.A., Boni, M.F., Chand, M., Choga, W.T., Colquhoun, R., Davids, M., Deforche, K., Doolabh, D., Du Plessis, L., Engelbrecht, S., Everatt, J., Giandhari, J., Giovanetti, M., Hardie, D., Hill, V., Hsiao, N.Y., Iranzadeh, A., Ismail, A., Joseph, C., Joseph, R., Koopile, L., Kosakovsky Pond, S.L., Kraemer, M.U.G., Kuate-Lere, L., Laguda-Akingba, O., Lesetedi-Mafoko, O., Lessells, R.J., Lockman, S., Lucaci, A.G., Maharaj, A., Mahlangu, B., Maponga, T., Mahlakwane, K., Makatini, Z., Marais, G., Maruapula, D., Masupu, K., Matshaba, M., Mayaphi, S., Mbhele, N., Mbulawa, M.B., Mendes, A., Mlisana, K., Mnguni, A., Mohale, T., Moir, M., Moruisi, K., Mosepele, M., Motsatsi, G., Motswaledi, M.S., Mphoyakgosi, T., Msomi, N., Mwangi, P.N., Naidoo, Y., Ntuli, N., Nyaga, M., Olubayo, L., Pillay, S., Radibe, B., Ramphal, Y., Ramphal, U., San, J.E., Scott, L., Shapiro, R., Singh, L., Smith-Lawrence, P., Stevens, W., Strydom, A., Subramoney, K., Tebeila, N., Tshiabuila, D., Tsui, J., Van Wyk, S., Weaver, S., Wibmer, C.K., Wilkinson, E., Wolter, N., Zarebski, A.E., Zuze, B., Goedhals, D., Preiser, W., Treurnicht, F., Venter, M., Williamson, C., Pybus, O.G., Bhiman, J., Glass, A., Martin, D.P., Rambaut, A., Gaseitsiwe, S., Von Gottberg, A., De Oliveira, T., 2022. Rapid epidemic expansion of the SARS-CoV-2 Omicron variant in southern Africa. Nature 603, 679–686.

Wei, C., Shan, K.J., Wang, W., Zhang, S., Huan, Q., Qian, W., 2021. Evidence for a mouse origin of the SARS-CoV-2 Omicron variant. J. Genet. Genomics 48, 1111–1121.

WHO, 2022a. WHO Coronavirus (COVID-19) Dashboard [Online]. World Health Organization. Available: https://covid19.who.int/. (Accessed 12 January 2022).

WHO, 2022b. Tracking SARS-CoV-2 variants [Online]. World Health Organization. Available: https://www.who.int/en/activities/tracking-SARS-CoV-2-variants/ [Accessed 12 January 2022].

Wrobel, A.G., Benton, D.J., Xu, P., Roustan, C., Martin, S.R., Rosenthal, P.B., Skehel, J.J., Gamblin, S.J., 2020. SARS-CoV-2 and bat RaTG13 spike glycoprotein structures inform on virus evolution and furin-cleavage effects. Nat. Struct. Mol. Biol. 27, 763–767.

Wu, C., Zheng, M., Yang, Y., Gu, X., Yang, K., Li, M., Liu, Y., Zhang, Q., Zhang, P., Wang, Y., Wang, Q., Xu, Y., Zhou, Y., Zhang, Y., Chen, L., Li, H., 2020. Furin: a potential therapeutic target for COVID-19. iScience 23, 101642.

Wu, L., Zhou, L., Mo, M., Liu, T., Wu, C., Gong, C., Lu, K., Gong, L., Zhu, W., Xu, Z., 2022. SARS-CoV-2 Omicron RBD shows weaker binding affinity than the currently dominant Delta variant to human ACE2. Signal Transduct. Target. Ther. 7, 8.

Xing, X., Wang, L., Cui, Z., Fu, W., Zheng, T., Qin, L., Ge, P., Qian, A., Wang, N., Yuan, S., 2022. Structures of SARS-CoV-2 spike protein alert noteworthy sites for the potential approaching variants. Virol. Sin. 37, 938–941.

Zhang, X., Wu, S., Wu, B., Yang, Q., Chen, A., Li, Y., Zhang, Y., Pan, T., Zhang, H., He, X., 2021. SARS-CoV-2 Omicron strain exhibits potent capabilities for immune evasion and viral entrance. Signal Transduct. Target. Ther. 6, 430.

Zhang, Y., Wei, M., Wu, Y., Wang, J., Hong, Y., Huang, Y., Yuan, L., Ma, J., Wang, K., Wang, S., Shi, Y., Wang, Z., Guo, H., Xiao, J., Yang, C., Ye, J., Chen, J., Liu, Y., Fu, B., Lan, M., Gong, P., Huang, Z., Su, Y., Chen, Y., Zhang, T., Zhang, J., Zhu, H., Yu, H., Yuan, Q., Cheng, T., Guan, Y., Xia, N., 2022a. Cross-species tropism and antigenic landscapes of circulating SARS-CoV-2 variants. Cell Rep. 38, 110558.

Zhang, Y., Zhang, T., Fang, Y., Liu, J., Ye, Q., Ding, L., 2022b. SARS-CoV-2 spike L452R mutation increases Omicron variant fusogenicity and infectivity as well as host glycolysis. Signal Transduct. Target. Ther. 7, 76.

Zhao, H., Lu, L., Peng, Z., Chen, L.L., Meng, X., Zhang, C., Ip, J.D., Chan, W.M., Chu, A.W., Chan, K.H., Jin, D.Y., Chen, H., Yuen, K.Y., To, K.K., 2022. SARS-CoV-2 Omicron variant shows less efficient replication and fusion activity when compared with Delta variant in TMPRSS2-expressed cells. Emerg. Microbes Infect. 11, 277–283.

Zheng, L., Wang, K., Chen, M., Qin, F., Yan, C., Zhang, X.E., 2022. Characterization and function of glycans on the spike proteins of SARS-CoV-2 variants of concern. Microbiol. Spectr. 10, e0312022.

Starr, T.N., Greaney, A.J., Hilton, S.K., Ellis, D., Crawford, K.H.D., Dingens, A.S., Navarro, M.J., Bowen, J.E., Tortorici, M.A., Walls, A.C., King, N.P., Veesler, D., Bloom, J.D., 2020. Deep mutational scanning of SARS-CoV-2 receptor binding domain reveals constraints on folding and ACE2 binding. Cell 182, 1295–1310.e20.